Journal of Nuclear Materials 396 (2010) 57–64

Contents lists available at ScienceDirect

Journal of Nuclear Materials

journal homepage: www.elsevier.com/locate/jnucmat

Compatibility of ferritic–martensitic steel T91 welds with liquid lead–bismuth eutectic: Comparison between TIG and EB welds

J. Van den Bosch [a,b,c,*], G. Coen [a], W. Van Renterghem [b], A. Almazouzi [b]

[a] UGent, Department of Materials Science and Engineering, St. Pietersnieuwstraat 41, B-9000 Ghent, Belgium
[b] SCK•CEN (Belgian Nuclear Research Centre), Boeretang 200, B-2400 Mol, Belgium
[c] Los Alamos National Laboratory, P.O. Box 1663, Los Alamos, NM 87545, USA

ARTICLE INFO

Article history:
Received 12 June 2009
Accepted 20 October 2009

ABSTRACT

The 9 wt.% chromium ferritic–martensitic steel T91 is being considered as candidate structural material for a future experimental accelerator driven system (XT-ADS). This material and its welded connections would need to be used in contact with liquid lead–bismuth eutectic (LBE), under high irradiation doses. Both unirradiated tungsten inert gas (TIG) and electron beam (EB) welds of T91 have been examined by means of metallography, scanning electron microscopy (SEM-EDX), transmission electron microscopy (TEM), Vickers hardness measurements and tensile testing in both gas and liquid lead–bismuth environment. The TIG weld was commercially produced and post weld heat treated by a certified welding company while the post weld heat treatment of the experimental EB weld was optimized in terms of the Vickers hardness profile across the welded joint. The mechanical properties of the T91 TIG and EB welds in contact with LBE have been examined using slow strain rate tensile testing (SSRT) in LBE at 350 °C. All welds showed good mechanical behaviour in gas environment but total elongation was strongly reduced due to liquid metal embrittlement (LME) when tested in liquid lead–bismuth eutectic environment. The reduction in total elongation due to LME was larger for the commercially TIG welded joint than for the EB welded joint.

1. Introduction

In modern society, the welding procedure is one of the most important connection techniques available for metallic components. An incredibly wide variety of utensils and structures from the most simple, such as a spoon, to the most complicated, like off-shore platforms, ships or even nuclear reactors, could only be realised by application of one or several welds. It is therefore vital in the development of new materials and applications to optimize and qualify the welding procedure.

One nuclear system that has received a lot of attention lately is the accelerator driven system (ADS) [1,2]. It is proposed as one of the possible solutions to reduce the high level radio-active waste by transmuting the long lived actinides resulting from the fission reactor's spent fuel. The ADS technology however requires severe operating conditions. The structural materials and their welds need to withstand temperatures ranging between 200 and 550 °C under high neutron flux (>10^{14} neutrons cm^{-2} s^{-1}) while in contact with heavy liquid lead–bismuth eutectic metal.

Within the FP6 EUROTRANS-Demetra project, the ferritic–martensitic steel T91 and the austenitic stainless steel 316L were chosen as the reference candidate structural materials for the construction of the European ADS under study. These high chromium steels will need to be welded (both similar and dissimilar welds) successfully and need to withstand the stringent conditions similar to those to which the base materials will be subjected. The increased susceptibility of the T91/316L mixed TIG and EB welds to liquid metal embrittlement (LME) has been reported in an earlier paper [3]. LME of welded components could therefore be a critical issue and needs to be examined thoroughly.

Although welding high chromium steels has become a well known technique which is extensively used in the conventional power industry, the performance of high Cr and Cr–Mo steel welds is still often considered to be a life limiting factor at high temperatures. In fact, a high percentage of failures in the power industry have been reported to be welding related [4]. Furthermore, despite the extensive experience built up in welding high chromium steels, many of the certified welding procedures were developed for specific applications and the environmental conditions of new applications may strongly affect the weld. For instance, high Ni containing alloys are often used as filler material because of the high toughness of the resulting weld. These filler materials however need to be avoided when the weld is to be used in contact

* Corresponding author. Address: UGent, Department of Materials Science and Engineering, St. Pietersnieuwstraat 41, B-9000 Ghent, Belgium. Tel.: +32 (0)14 33 31 77; fax: +32 (0)14 32 12 16.
E-mail address: jvdbosch@sckcen.be (J. Van den Bosch).

0022-3115/$ - see front matter © 2009 Elsevier B.V. All rights reserved.
doi:10.1016/j.jnucmat.2009.10.054

with liquid heavy metals, such as Pb or LBE, due to the relatively high solubility of Ni in Pb and especially in PbBi.

Within the FP5 Spire project and in the frame of MEGAPIE (Megawatt Pilot Target Experiment) the importance of examining welds of T91 and 316L(N) was recognised and some irradiations were performed in the Swiss spallation neutron source (SINQ) [5,6] under atmosphere as well as in contact with LBE [7]. Experiments designed for fast breeder and fusion reactors have also produced interesting results on welds which could be very useful for an ADS system, such as the investigation of EB and TIG welded ferritic–martensitic steel EM10 to relatively high doses [8] and the reweldability studies on 316L(N) [9]. However, due to the complex nature of welds and the variety of welding procedures, applicable data needs to be rather specific and is therefore usually scarce.

In this paper, we discuss the susceptibility of T91/T91 welds to liquid metal embrittlement when in contact with liquid lead–bismuth eutectic by comparing two types of weld tested in gas and liquid metal environment. First, the technical information on the welding process of each of the examined welds is presented as well as the applied post weld heat treatment (PWHT) in the case of the TIG welded joints. Afterwards the microstructure and mechanical behaviour of the T91/T91 TIG and EB welds are looked at in detail and finally the tensile properties of the welds are compared when tested in liquid lead–bismuth eutectic environment.

2. Experimental

2.1. Materials

Two types of welds of the ferritic–martensitic steel T91 have been examined. The first weld was obtained by tungsten inert gas (TIG) welding in combination with shielded metal arc welding (SMAW) and submerged arc welding (SAW). The second weld type was obtained by electron beam (EB) welding. The chemical compositions of the ferritic–martensitic steel T91 base material and the TIG weld filler material (Thermanit MTS 3) used for the welds are given in Table 1. The chemical composition of the welding flux used for SAW is given in Table 2. The thermodynamic data important to the welding process of T91, as well as the yield strength, tensile strength and uniform and total elongation at room temperature in inert environment are summarized in Table 3. The T91 steel plate used as base material was fully characterized to assure the production of high quality welds [10]. The T91/T91 TIG weld was provided by the qualified welding company CMI, Belgium according to our specifications. The experimental electron beam welds were produced by Forschungszentrum Karlsruhe (FZK), Germany and were provided in the as welded condition.

2.1.1. T91/T91 TIG

The T91/T91 TIG weld comprises in total of 10 weld passes and is schematically represented in Fig. 1. The first two passes were performed using manual gas tungsten inert gas welding (GTAW) while applying a minimal preheating temperature of 220 °C. Passes 3–6 were performed by manual shielded metal arc welding (SMAW) with a minimal preheating temperature of 220 °C and weld passes 7–10 were done by submerged arc welding (SAW) under a bed of Marathon 543 flux (see Table 2) with a preheating temperature of minimum 230 °C.

Table 2
Chemical composition of the SAW flux material (Marathon 543), wt.%.

Material	CaF_2	$SiO_2 + TiO_2$	CaO + MgO	Al_2O_3 + MnO	$K_2O + Na_2O$
Marathon 543	31.0	14.0	32.0	18.0	2.6

The PWHT consisted of a maximum heating rate of 105 °C per hour up to 750 °C where the material was kept for 1 h and 10 min. The applied cooling rate was 100 °C per hour down to a temperature of 80 °C. At that moment, the welded plate was removed from the furnace and cooled down to ambient temperature without temperature control.

2.1.2. T91/T91 EB

The electron beam weld was performed by FZK in a single pass using an EBW 1001/10-60 CNC from PTR Präzisiontechnik, Maintal, Germany. The T91/T91 EB weld is schematically represented in Fig. 1. The vacuum chamber of the EB welding device used has a dimension of 580 mm by 350 mm with a height of 500 mm. Prior to EB welding, the plates to be welded were degreased and fixed together at a few points by manual TIG welding. When placed in the vacuum chamber, the chamber was pumped down to about 6×10^{-3} mbar. The electrical tension applied during EB welding for the EB weld under investigation was 60 kV, at a current of 62 mA. The welding speed was 10 mm s^{-1}. The T91/T91 EB weld was obtained in the as welded condition.

2.2. Sample preparation

For metallography, SEM and hardness measurements, a cross sectional beam of about 20 mm × 10 mm × 100 mm was cut out of the welded plate using a band saw. The large parallel surfaces of the T91/T91 weld specimens (see schematic representation in Fig. 1) were mechanically polished on a Struers Rotopol-11 using SiC paper followed by diamond suspension on cloth with particle sizes down to 1 μm. Etching of the T91 welds was done using Villella's reagent.

After visualisation of the different zones of the welds by polishing and etching, 3 mm diameter cylinders were cut out of the heat affected zones and out of the weld deposit for both the T91/T91 TIG and T91/T91 EB welds. From these cylinders TEM specimens were cut, mechanically polished and prepared by electrochemical polishing.

Cylindrical tensile specimens with a total length of 24 mm, a gauge length of 12 mm and a diameter of 2.4 mm were taken along different orientations of the T91/T91 TIG weld (across the weld with the weld deposit in the centre of the specimen gauge, across the weld with the HAZ in the centre of the gauge and parallel to the weld inside the weld deposit) and across the T91/T91 EB weld (weld zone in centre of gauge). The specimen's gauges were polished up to a P#4000 fine grid.

After tensile testing in liquid lead–bismuth eutectic environment samples were cleaned using a chemical solution of hydrogen peroxide, acetic acid and ethanol in a ratio of 1:1:1.

Table 1
Chemical composition of the T91 base material and the weld deposit material (Thermanit MTS 3), wt.%.

Material	B	C	N	Al	Si	P	S	V	Cr	Mn	Ni	Cu	Nb	Mo
T91	<1 wppm	0.1	0.04	0.01	0.22	0.021	0.0004	0.21	8.99	0.38	0.11	0.06	0.06	0.89
Thermanit MTS 3	<1 wppm	0.130	0.04	0.009	0.24	0.004	0.004	0.186	9.00	0.56	0.66	0.04	0.05	0.98

Table 3
Thermodynamic and mechanical data of T91.

Melting temperature (K)	Thermal conductivity[a] ($W\,m^{-1}\,K^{-1}$)	Thermal expansion coefficient[a] ($10^{-6}\,K^{-1}$)	Specific heat ($J\,kg^{-1}\,K^{-1}$)	Latent heat of fusion ($J\,kg^{-1}$)	Yield strength[a] ($\sigma_{0.2}$) (MPa)	Tensile strength[a] (σ_{UTS}) (MPa)	Total elongation[a] (ε_{tot}) (%)	Uniform elongation[a] (ε_{unif}) (%)
1773	22.1	10.4	444.8	2.6×10^5	580	708	21	6.6

[a] At room temperature.

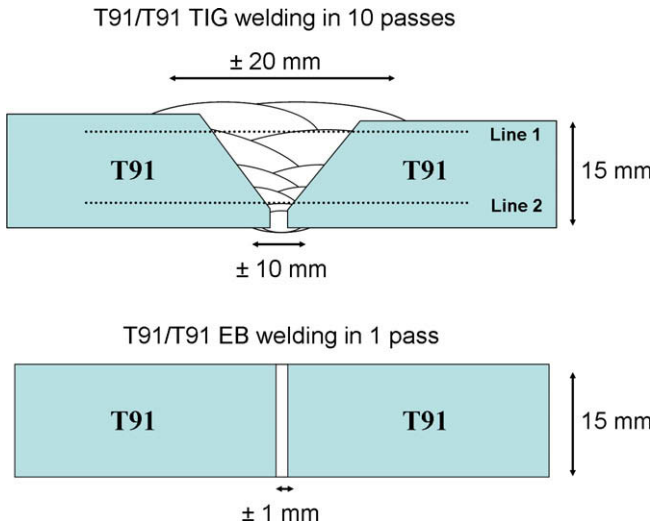

Fig. 1. Schematic representation of T91/T91 TIG and T91/T91 EB welds.

3. Results and discussion

Fig. 2 shows the microstructures of both the T91/T91 TIG weld (Fig. 2A) and the T91/T91 EB weld (Fig. 2B). Due to the different widths of the weld seam, the TIG weld is only partially visible while the entire EB weld is shown in Fig. 2.

Based on the optical microscopy, both the T91/T91 TIG and EB welds show a fully martensitic lath microstructure. After etching, the different welding passes of the TIG weld can clearly be distinguished. In Fig. 2A, two weld passes are partially shown and are indicated by a dashed line separating the individual passes. The evolution of grain sizes due to the different temperatures obtained in the HAZ of the TIG weld is difficult to distinguish. However, as in ferritic welds, the HAZ has the characteristic morphology of a grain growth region close to the weld interface and a grain refined region farther away from the weld interface [5]. The upper left in Fig. 2A shows the TIG weld whereas the lower right bottom of the picture shows the microstructure of the base material. The EB weld in contrast to the TIG weld can be kept relatively small due to the process of electron beam welding. Note that the total width of the EB weld and heat affected zone of this 15 mm thick welded plate is only a few millimetres as can be seen in Fig. 2B. The heat affected zone of this type of welds is therefore very small and differences in grain size between the grains in the HAZ on the side of the base material and the grain size in the HAZ on the side of the weld can be kept to a minimum. No porosity, micro-cracks or large slag inclusions were found by optical microscopy in either welded joint.

The EB weld is expected to have significantly smaller influence on the mechanical behaviour of the material compared to a traditional TIG weld due to the narrow weld and the constant chemical composition across the weld. The chemical composition of the EB welded joint as measured by EDX does not vary across the weld and the measured scatter in chemical composition of the weld shown in Fig. 3B is similar in the base material. The composition of the TIG welded joint however does vary slightly across the weld and the weld seam is generally over alloyed compared to the base material. This is illustrated in Fig. 3A which shows the composition profile across the TIG weld.

As stated before, the final interest of this work was the mechanical behaviour of the welded joints in liquid lead–bismuth eutectic (LBE). However, the quality of the welds needed to be assured mechanically before being able to draw conclusions on any possible tests in LBE. Therefore, Vickers hardness measurements, using a 5 kg force, were performed across both types of welded joints to assure their quality. The hardness indentations across the T91/T91 TIG welded joint were made both on the upper, wider side of the V-shaped weld as well as on the lower, narrower side which is indicated respectively by line 1 and line 2 in Fig. 1. Note that the TIG weld had been given a proper heat treatment at the welding company as mentioned earlier. The hardness profile after PWHT of the T91/T91 TIG weld seam has the typical hardness dip in the fine grained region of the HAZ close to the base material (intercritical zone) as can be seen in Fig. 4. This softened zone in a weld is usually very thin. Nevertheless it determines the creep rupture strength of the weld when transverse stresses are dominant. Under such conditions, the supporting effect of neighboring regions with higher strength decreases more and more as the operating time increases and the fracture mode becomes increasingly intergranular. Therefore, cross weld creep tests of T91 show a shift in fracture location from the base material to the fine grained HAZ. This phenomenon is known as type IV cracking and the shift in fracture location is stress and temperature dependent [11]. Notice however that such a decrease in creep rupture strength is of importance only when the principle stress is acting in cross weld direction. The hardness values across the T91/T91 TIG weld do correspond to the expected values for this type of weld and therefore confirm the quality of the performed weld and subsequent PWHT [12].

As mentioned earlier the T91/T91 electron beam weld was supplied in the as welded condition and needed to be given an appropriate PWHT. The optimal PWHT consisted of a heating ramp of 100 °C per hour and a holding time of 1 h 10′ at 750 °C. Longer holding times tended to increase softening of the base material, whereas shorter holding times resulted in a smaller decrease of the hardness peak. The cooling was done at a maximum rate of 100 °C per hour. The results of the Vickers hardness measurements across the electron beam weld before and after PWHT are depicted in Fig. 4.

Due to the applied PWHT the hardness maximum of the T91/T91 EB weld was decreased from 466 to 283 H_v and corresponds to the values found for the T91/T91 TIG weld without significantly softening the base material. Again, the hardness profile after PWHT of the EB welded T91/T91 seam has the typical hardness dip in the fine grained region of the HAZ close to the base material (intercritical zone) as can be seen in Fig. 4. Note that the width of the zone influenced by the EB weld also narrowed due to the PWHT. This was thought to be the optimum post weld heat treatment for this welded joint.

The microstructure of the heat affected zone and of the weld deposit was investigated by TEM for both the T91/T91 TIG and EB

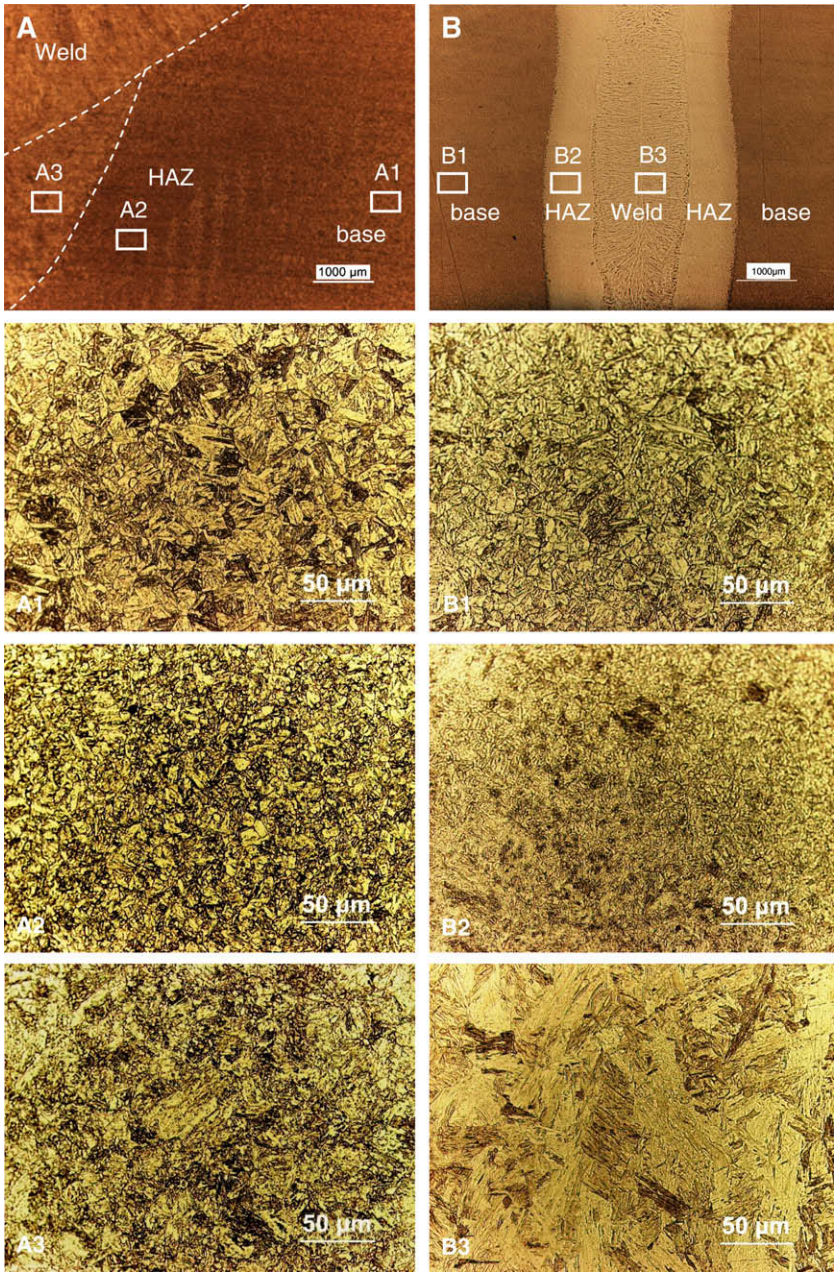

Fig. 2. Optical microscopy images of (a) The T91/T91 TIG; (b) The T91/T91 EB weld showing the weld seam, heat affected zone (HAZ) and base material.

welds. Because the TIG weld received the PWHT at the welding company, its microstructure could only be looked at after PWHT. For the T91/T91 EB weld however, the HAZ and weld deposit were examined before and after PWHT. The obtained TEM images are depicted in Fig. 5. The HAZ of the T91/T91 TIG weld revealed a very similar microstructure as in the base material, having $M_{23}C_6$ carbides of similar size on the lath boundaries and VC and NbC precipitates inside the martensite laths. In the T91/T91 TIG weld deposit (see Fig. 5A and B), apart from the $M_{23}C_6$ precipitates at the lath boundaries and the MC precipitates inside grains, some oxide particles were found as well. These particles were spherical in shape and had sizes up to approximately 1 µm. Based on the EDX spectrum analysis, these particles consisted mainly of Al_2O_3 and SiO_2 and most likely originated from the welding flux. Certain grains in the T91/T91 TIG weld deposit showed very clear dislocation substructures (see dark field image Fig. 5B) and where VC or NbC particles were found, dislocations were pinned on these precipitates. In the as welded T91/T91 EB weld, no precipitates were found as can be seen in the bright field image overview of Fig. 5C. Moreover, the fused zone of the EB weld also had a very high dislocation density, (see dark field image Fig. 5D) which indicates a rapid solidification and cooling rate of the molten zone of the weld. Both the over saturated solid solution caused by the solution of precipitates during welding followed by rapid solidification and cooling and the thereby created very high dislocation density, contribute to the hardness increase of the EB weld observed in Fig. 4. The HAZ, on the other hand, contains the expected $M_{23}C_6$ precipitates on the lath boundaries as well as the VC and NbC inside the martensite laths after EB welding as can be seen in Fig. 5E. Certain grains of the EB weld HAZ still have a rather high dislocation density as shown in the dark field image of Fig. 5F. However, these higher dislocation density grains do show dislocation structure formation

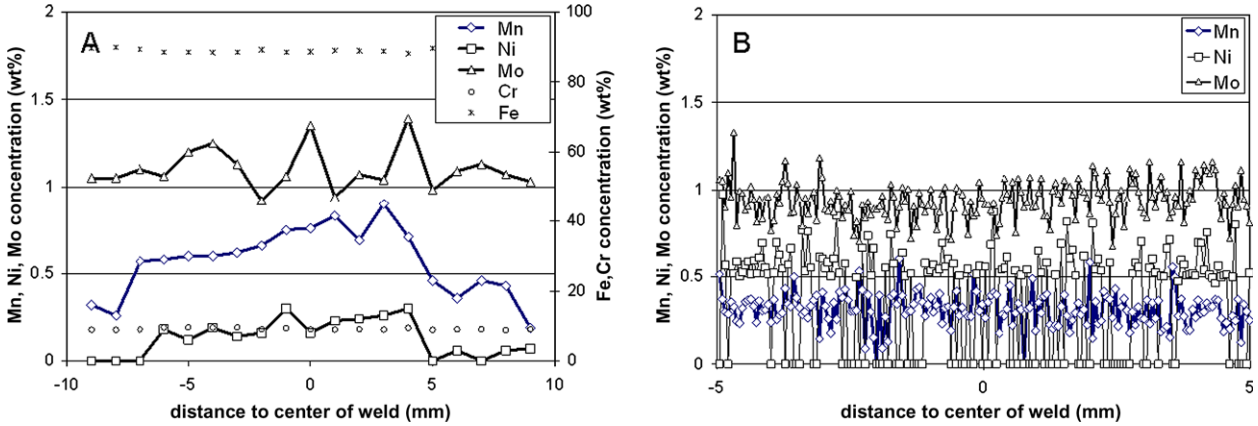

Fig. 3. Chemical composition across the weld. (A) Mn, Ni, Mo (left scale) and Fe, Cr (right scale) content across the T91/T91 TIG weld (1 mm distance between EDX measuring points); (B) Mn, Ni, Mo content across the T91/T91 EB weld.

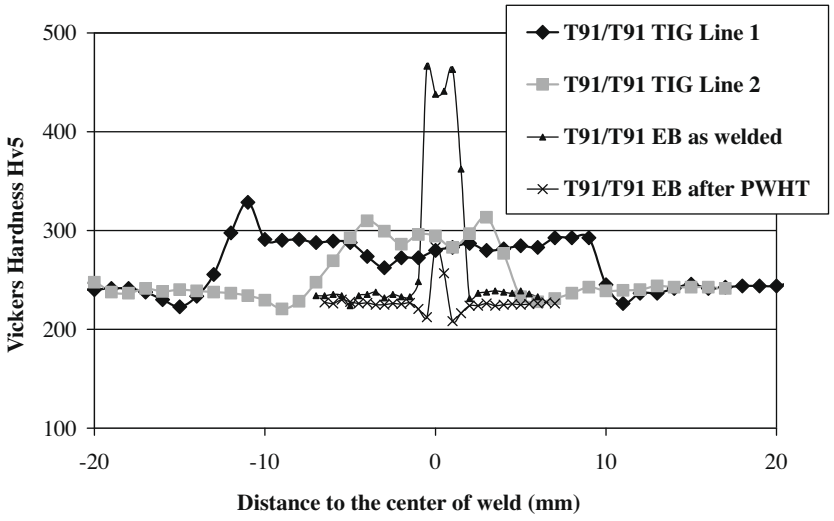

Fig. 4. Vickers hardness profile across the T91/T91 EB weld before and after post weld heat treatment and across the T91/T91 TIG weld near the wide weld surface (see line 1 in Fig. 1) and near the narrow weld surface (see line 2 in Fig. 1).

similar to the T91/T91 TIG weld after PWHT (see Fig. 5B). After post weld heat treatment, the EB weld fusion zone does contain the expected $M_{23}C_6$ carbides on the grain and lath boundaries and smaller VC and NbC carbides inside the martensite laths (see Fig. 5G). Furthermore, the PWHT caused the dislocation density inside the EB weld zone to decrease significantly and to form dislocation cell structures. This can clearly be seen by comparing the dislocation structure shown in the bright field image of Fig. 5H to the random, high dislocation density in Fig. 5D. In the HAZ of the EB weld, the PWHT caused the dislocation cell structure to become more dominant, forming dislocation cells that no longer contain dislocations inside them (see Fig. 5J) which contributes to the hardness dip observed in the HAZ of the EB weld after PWHT.

Increased hardness is known to strongly increase the susceptibility of ferritic–martensitic steels to LME in liquid lead–bismuth eutectic environment [13,14]. Therefore, the as welded T91/T91 EB weld was not tested in liquid LBE environment and mechanical testing was only performed on the T91/T91 welds after proper PWHT. Tensile tests were performed using a strain rate of $5 \times 10^{-6}\,s^{-1}$ at 350 °C in both gas (argon and 5% hydrogen mixture) and liquid lead–bismuth eutectic purged with an argon and 5% hydrogen gas mixture. The stress–strain curves are depicted in Fig. 6. The samples tested in LBE were pre-exposed in LBE with low oxygen concentration, following the thermal cycling pattern identical to the samples in the Twin Astir irradiation experiment [15]. This thermal cycling procedure involved exposure to six periods of approximately 1 month each at about 350 °C separated by periods of about 1 month at room temperature. Despite the fact that the hardness measurements presented in Fig. 4 for were performed prior to the exposure to low oxygen containing LBE under cycling thermal conditions, the Vickers hardness values are considered to be still valid for the exposed material. The exposure in LBE was to a maximum of 360 °C which is below the martensite start temperature (M_s) of the T91 steel. At these temperatures, none of the alloying elements have significant mobility in the material to cause any changes in the microstructure, even after 6 months of exposure. Furthermore, due to the PWHT at 750 °C for 1 h and 10 min, the glissile dislocations present in the microstructure will have just a minimal tendency to allow stress relaxation during exposure at 360 °C. The thermal ageing effect of the exposure is expected to be negligible and the results after exposure can be directly compared to those after PWHT. The pre-exposure to LBE under low oxygen concentration conditions is however considered to be beneficial to the wetting by the LBE [16].

Fig. 6 shows that both the T91/T91 TIG and EB welds have good mechanical behaviour when tested in gas environment. The tensile

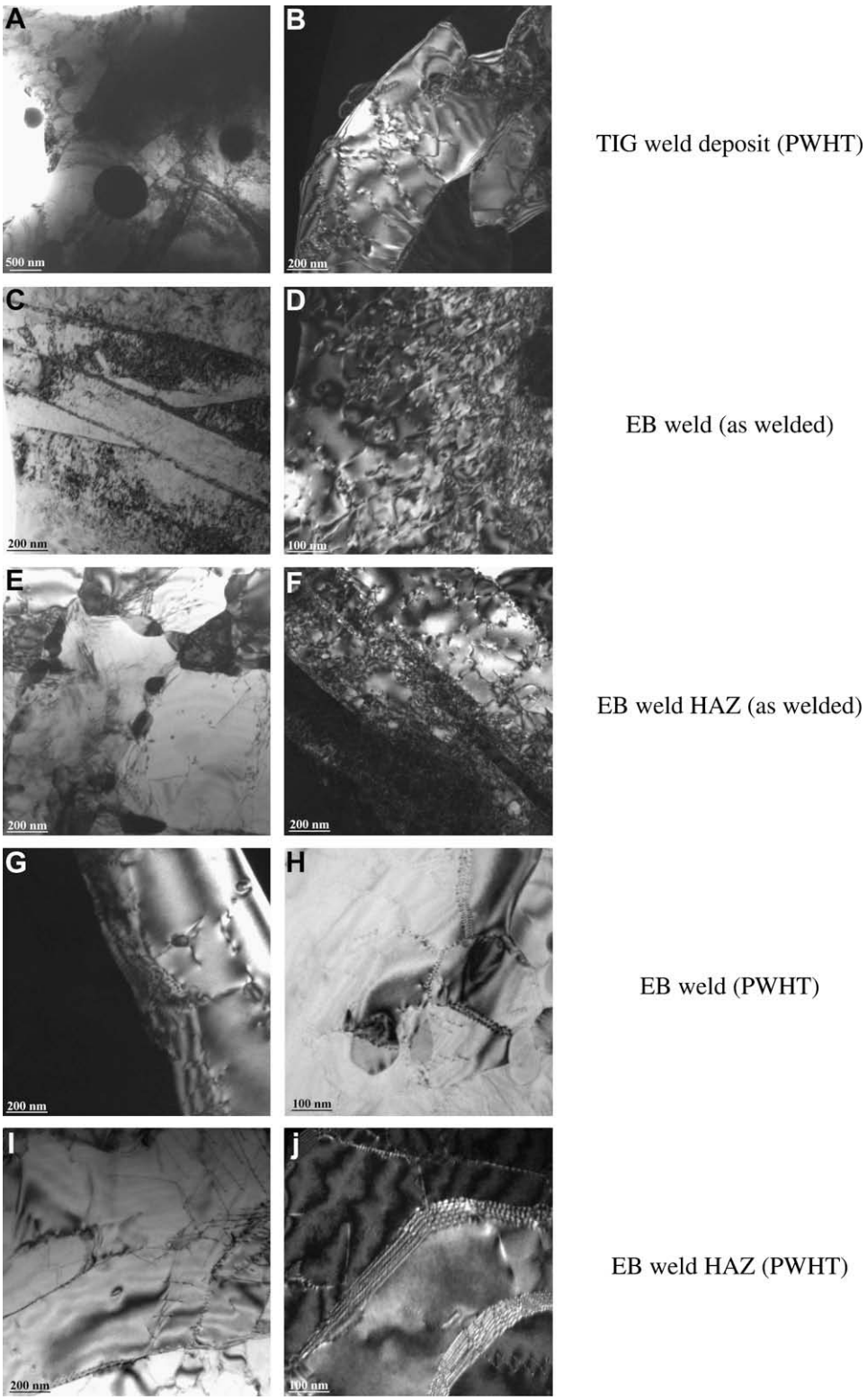

Fig. 5. TEM images of T91/T91 TIG (A, B) and EB (C–J) weld microstructure. (A) Bright field image of TIG weld deposit after post weld heat treatment; (B) Dark field image of TIG weld deposit after post weld heat treatment; (C) Bright field image of EB weld deposit; (D) Dark field image of EB weld deposit; (E) Bright filed image of EB weld heat affected zone; (F) Dark field image of EB weld heat affected zone; (G) Dark field image of EB weld deposit after post weld heat treatment; (H) Bright field image of EB weld deposit after post weld heat treatment; (I) Bright field image of EB weld heat affected zone after post weld heat treatment; (J) Dark field image of EB weld heat affected zone after post weld heat treatment.

curve of the T91 base material tested in gas environment under the same conditions was added to the EB weld data for comparison (see stress–strain curves on the right in Fig. 6). When tested in liquid lead–bismuth eutectic environment however, all welds showed significantly decreased total elongation. The elastic behaviour and yield point of both the T91/T91 TIG and EB welds were unaffected by the environment indicating no significant penetration of the LBE into the weld or matrix during pre-exposure. The

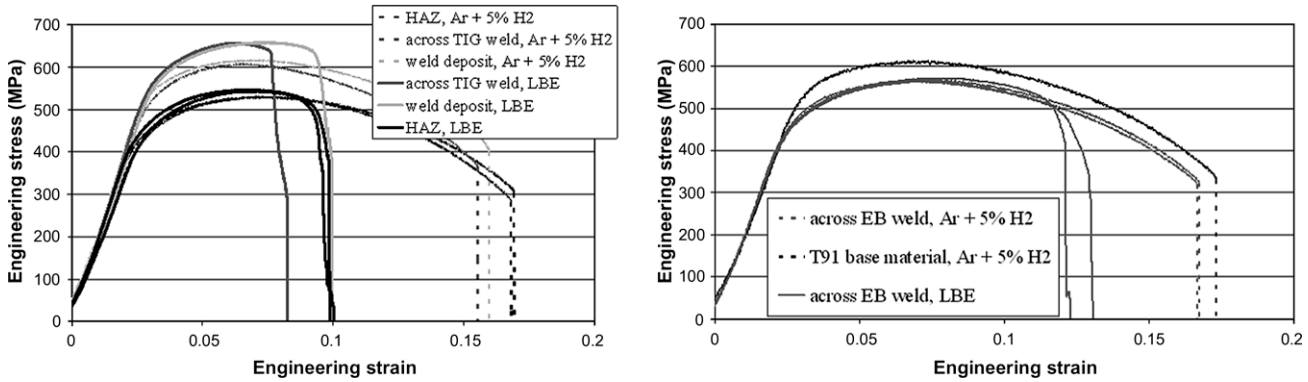

Fig. 6. Engineering stress–strain curves of (a) T91/T91 TIG weld; (b) T91/T91 EB weld along various orientations of the welds, tested in argon and hydrogen gas mixture (dashed curves) and in LBE (solid curves) at 350 °C, using a strain rate of 5×10^{-6} s^{-1}.

plastic behaviour of both weld types also remains the same up to the point of fracture. In the case of the T91/T91 TIG weld tested in liquid LBE, fracture followed shortly after reaching the ultimate tensile strength (see Fig. 6 on the left). The T91/T91 EB weld displayed higher total elongation when tested in liquid LBE however its total elongation was still significantly reduced compared to that of the T91/T91 EB weld tested in gas environment. This type of fracture behaviour is typically observed where liquid metal embrittlement occurs and follows the observations of Westwood et al. [17] who claim that the stress–strain behaviour of the solid metal is the same as in the unwetted condition until premature fracture occurs. Cross sectional Vickers hardness testing revealed that in all samples taken across the weld and tested in liquid LBE environment fracture occurred in an area of increased hardness. These areas of increased hardness correspond to the weld zones as shown in Fig. 4. The sample taken inside the weld deposit of the T91/T91 TIG weld fractured in the centre of the gauge.

Detailed SEM examination of the fracture surfaces revealed that all T91/T91 weld samples tested in gas environment (see left column in Fig. 7) were fully dimpled and showed the cup and cone shape characteristic of ductile failure. The SEM fracture surface images of the T91/T91 weld samples tested in liquid LBE are depicted in the middle column of Fig. 7. Detailed fracture surface images from the brittle regions of the specimens tested in LBE

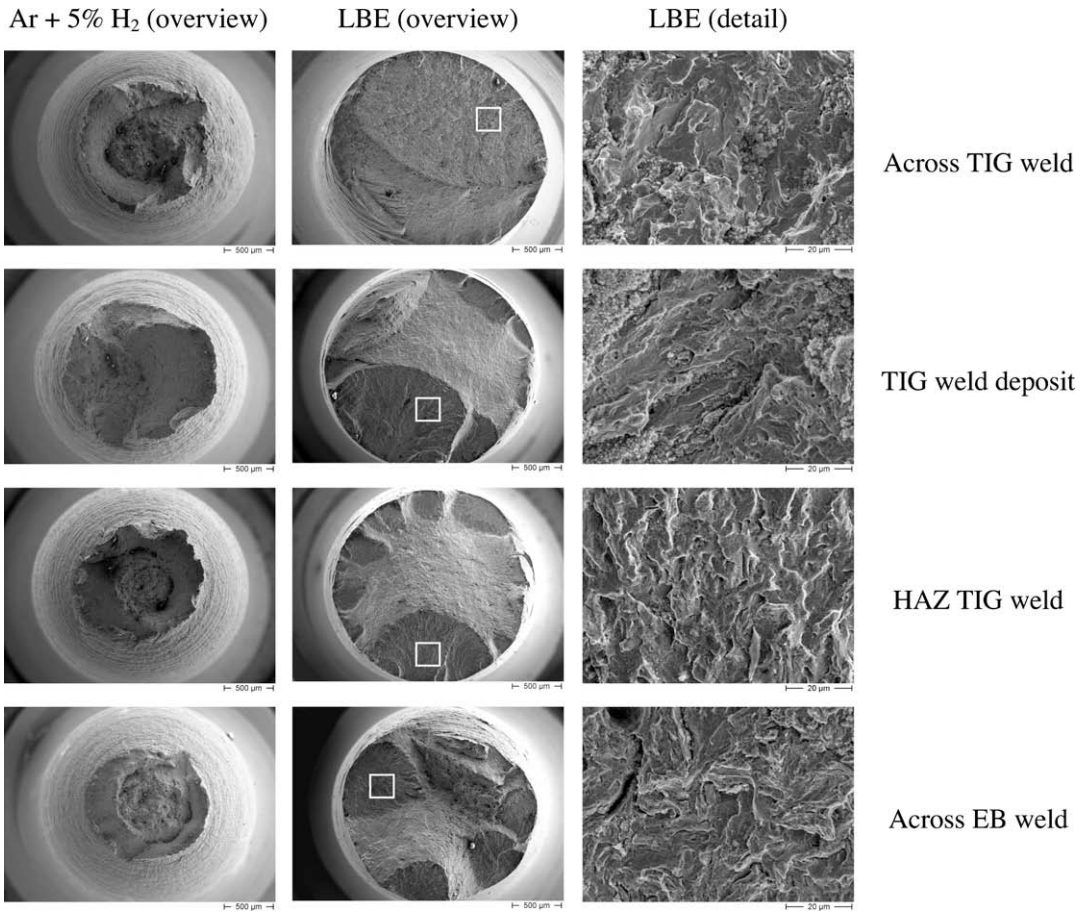

Fig. 7. SEM fracture surface images of T91/T91 TIG and T91/T91 EB weld samples along various orientations of the welds (indicated on the right), tested in argon and hydrogen gas mixture (left column) and in LBE (right column) at 350 °C, using a strain rate of 5×10^{-6} s^{-1}.

and indicated by a box in the overview SEM images are depicted on the right in Fig. 7. The weld specimens tested in liquid LBE showed very limited necking with the fracture surface perpendicular to the load line. All fracture surfaces of T91/T91 weld samples tested in liquid LBE show at least one initiation site of LME characterized by the semi-circular flower pattern as seen in LME studies of T91 base material [18,19].

4. Conclusions

Two types of welds of the ferritic–martensitic steel T91 were characterized and compared to assess the quality of the weld and its microstructure. Furthermore the mechanical behaviour of the T91/T91 welds was tested in both liquid lead–bismuth eutectic and in gas environment at 350 °C to compare the susceptibility to LME of the different types of welds. The studied welds were a T91/T91 TIG weld provided and heat treated by a certified welding company and a T91/T91 experimental electron beam weld which received a post weld heat treatment based on the optimization of the hardness profile across the weld. Both weld types were of good quality showing typical hardness values across the weld after post weld heat treatment and having tensile behaviour similar to that of the base material when tested in gas environment. However, when tested in liquid lead–bismuth eutectic environment the total elongation was strongly reduced due to liquid metal embrittlement. The reduction in total elongation due to LME was larger for the commercially TIG welded joint than for the EB welded joint under the test conditions applied in this study.

Acknowledgements

Special thanks to I. Serre and J.-B. Vogt (CNRS, France) for the in depth constructive discussions on the examined welds and to S.A. Maloy (LANL, USA) for his critical review of this paper.

This work was partly supported by the European project IP-EUROTRANS-DEMETRA under contract No. FI6W-CT-2004-516520.

References

[1] L. Cinotti, B. Giraud, H. A Abderrahim, J. Nucl. Mater. 335 (2004) 148–155.
[2] H. A Abderrahim, P. Kupschus, E. Malambu, Ph. Benoit, K. Van Tichelen, B. Arien, F. Vermeersch, P. D'hondt, Y. Jongen, S. Ternier, D. Vandeplassche, Nucl. Instr. Meth. Phys. Res. A 463 (2001) 487–494.
[3] J. Van den Bosch, A. Almazouzi, J. Nucl. Mater. 385 (2009) 504–509.
[4] Baldev Raj, B.K. Choudhary, R.K. Singh Raman, Int. J. Press. Vess. Piping 81 (2004) 521–534.
[5] X. Jia, Y. Dai, J. Nucl. Mater. 343 (2005) 212–218.
[6] D. Hamaguchi, Y. Dai, J. Nucl. Mater. 343 (2005) 262–266.
[7] H. Glasbrenner, Y. Dai, F. Gröschel, J. Nucl. Mater. 343 (2005) 267–274.
[8] A. Alamo, J.L. Séran, O. Rabouille, J.C. Brachet, A. Maillard, H. Touron, J. Royer, in: Effects of Radiation on Materials: 17th International Symposium, ASTM STP 1270, 1996, pp. 761–774.
[9] H. Yamada, H. Kawamura, K. Tsuchiya, G. Kalinin, W. Kohno, Y. Morishima, J. Nucl. Mater. 307–311 (2002) 1584–1589.
[10] J. Van den Bosch, A. Almazouzi, Procurement and Characterization of T91 and SS316L plates, Scientific Report EUROTRANS-Demetra, R-4197, 2005.
[11] C.J. Middleton, J.M. Brear, R. Munson, R. Viswanathan, in: Advances in Materials Technology for Fossil Power Plants, Proceedings of the 3rd Conference held at University of Wales Swansea, 5th–6th April 2001, 2001, pp. 69–78.
[12] K. Coleman, D. Gandy, Guideline for Welding P(T)91, Document 1006590, EPRI, 1300 W.T. Harris Blvd., Charlotte, NC 28262, USA, 2002.
[13] A. Legris, G. Nicaise, J.-B. Vogt, J. Foct, D. Gorse, D. Vançon, Scr. Mater. 43 (11) (2000) 997–1001.
[14] T. Sample, H. Kolbe, J. Nucl. Mater. 283–287 (2000) 1336–1340.
[15] J. Van den Bosch, A. Al Mazouzi, Ph. Benoit, R.W. Bosch, W. Claes, B. Smolders, P. Schuurmans, H. A Abderrahim, J. Nucl. Mater. 377 (2008) 206–212.
[16] J. Van den Bosch, D. Sapundjiev, A. Almazouzi, J. Nucl. Mater. 356 (2006) 237–246.
[17] A.R.C. Westwood, C.M. Preece, M.H. Kamdar, in: Adsorption Induced Brittle Fracture in Liquid Environments, vol. 3, Academic Press, 1971, p. 589.
[18] J. Van den Bosch, G. Coen, A. Almazouzi, J. Degrieck, J. Nucl. Mater. 385 (2) (2009) 250–257.
[19] F. Di Gabriele, A. Doubková, A. Hojná, J. Nucl. Mater. 376 (2008) 307–311.